Article

Targeting endothelin receptors in a murine model of myocardial infarction using a small molecular fluorescent probe

Melanie A. Kimm, Helena Haas, Miriam Stölting, Michael Kuhlmann, Christiane Geyer, Sarah Glasl, Michael Schäfers, Vasilis Ntziachristos, Moritz Wildgruber, and Carsten Höltke

Mol. Pharmaceutics, **Just Accepted Manuscript** • DOI: 10.1021/acs.molpharmaceut.9b00810 • Publication Date (Web): 09 Dec 2019

Targeting endothelin receptors in a murine model of myocardial infarction using a small molecular fluorescent probe

Melanie A. Kimm[1], Helena Haas[1], Miriam Stölting[2], Michael Kuhlmann[3], Christiane Geyer[2], Sarah Glasl[4], Michael Schäfers[3], Vasilis Ntziachristos[4], Moritz Wildgruber[1,2,*], Carsten Höltke[2,*,†]

1) Department of Diagnostic and Interventional Radiology, School of Medicine and Klinikum rechts der Isar, Technical University of Munich, Munich, Germany; 2) Translational Research Imaging Center, Department of Clinical Radiology, University Hospital Münster, Münster, Germany; 3) European Institute for Molecular Imaging, University Hospital Münster, Münster, Germany; 4) Institute of Biological and Medical Imaging, Helmholtz Zentrum München, Munich, Germany.

Abstract. The endothelin-(ET-)axis plays a pivotal role in cardiovascular diseases. Enhanced levels of circulating ET-1 have been correlated with inferior clinical outcome after myocardial infarction (MI) in humans. Thus, the evaluation of endothelin-A receptor (ET_AR) expression over time in the course of myocardial injury and healing may offer valuable information towards the understanding of ET-axis involvement in MI. We developed an approach to track the expression of ET_AR with a customized molecular imaging probe in a murine model of MI. The small molecular probe based on the ET_AR selective antagonist 3-(1,3-Benzodioxol-5-yl)-5-hydroxy-5-(4-methoxyphenyl)-4-[(3,4,5-tri-methoxyphenyl)methyl]-2(5*H*)-furanone (PD156707) was labelled with fluorescent dye IRDye800cw. Mice undergoing permanent ligation of the left anterior descending artery (LAD) were investigated at day 1, 7 and 21 post surgery after receiving an i.v. injection of the ET_AR probe. Cryosections of explanted hearts were analyzed by cryotome-based CCD and fluorescence reflectance imaging (FRI) and fluorescence signal intensities (SI) were extracted. Fluorescence mediated tomography (FMT) imaging was performed to visualize probe distribution in the target region *in vivo*. Enhanced fluorescence signal intensity in the infarct area was detected in cryoCCD images as early as day 1 after surgery and intensified up to 21 days post MI. FRI was capable of detecting significantly enhanced SI in infarcted regions of hearts 7 days after surgery. *In vivo* imaging by FMT localized enhanced SI in the apex region of infarcted mouse hearts. We verified localization of probe and ET_AR within the infarct area by immunohistochemistry (IHC). In addition, neovascularized areas were found in the affected myocardium by CD31 staining. Our study demonstrates that the applied fluorescent probe is capable of delineating ET_AR expression over time in affected murine myocardium after MI *in vivo* and *ex vivo*.

Keywords: Endothelin Axis, Myocardial Infarction, Molecular Imaging, Optical Imaging

* equal contribution
† corresponding author

Introduction:

The endothelin-(ET-) system consists of three 21-amino acid peptides, ET-1, -2 and -3 and two associated G-protein-coupled receptors. The endothelin-A (ET_AR) and endothelin-B (ET_BR) receptors are widely distributed in mammalian organs, including heart and vasculature, adrenal gland and peripheral neurons, and are increasingly expressed in a number of human cancers. In the vasculature ET-1 is the main isoform. It is produced by endothelial cells, vascular smooth muscle cells, cardiomyocytes, macrophages and fibroblasts. Generally, signaling of ET-1 via ET_AR results in long-lasting vasoconstriction while stimulation of ET_BR leads to release of vasodilators such as prostaglandins and nitric oxide. Very early after the characterization and identification of ET-1 in the late 1980s[1, 2] its significance in cardiovascular (patho)physiology has been described. In pathologic conditions like chronic heart failure (CHF) ET-1 signaling leads to positive myocardial inotropy, arrhythmogenesis, an acceleration of cardiac hypertrophy and growth of cardiac fibroblasts.[3-7] Increased plasma ET-1 levels have been found in animal models of myocardial infarction (MI).[8-10] In clinical investigations, elevated levels of ET-1 and related peptides shortly after acute MI positively correlated with infarct size and served as a prognostic factor for survival rates.[5, 11-18] In mammals, both ET_AR and ET_BR expression is found throughout the cardiac muscle, including the coronary vasculature. Cardiomyocytes express predominantly ET_AR while both receptors are present on cardiac fibroblasts.[6, 19, 20] In cardiovascular pathologies ET receptors have been found to be up- as well as down-regulated, and the largest effects are described for ET_AR.[21-25] Treatment with ET receptor antagonists in a rat model of myocardial infarction have revealed beneficial effects when these were given delayed after MI, but detrimental effects when applied immediately post MI.[26-29] A number of endothelin receptor antagonists gave promising results in treatment of diverse cardiovascular diseases such as pulmonary arterial hypertension (PAH), atherosclerosis as well as heart and renal failure.[30-34] However, results are often contradictory and elaborated clinical trials with intravenous tezosentan, an unspecific ET_AR/ET_BR antagonist, ended with disappointing results.[35, 36] All these findings emphasize the importance of the endothelin axis in the realm of myocardial pathologies. Only few clinical trials showed benefit when blocking ET action in disease and the only FDA approved compounds are the mixed ET_AR/ET_BR antagonists Macitentan and Bosentan and the ET_AR-selective drug Ambrisentan; all of these are approved for the treatment of PAH.[3, 4, 37] In the setting of MI it seems unclear, when and how manipulation of the ET-axis improves clinical outcome. Yet, it is unclear, if addressing ET_AR or ET_BR (or both) would result in desirable beneficial effects.[6, 11] For a more detailed understanding of the acute physiological and chronic pathological effects of ET-signaling in cardiovascular disease, especially myocardial infarction, the knowledge about distribution and localization of ET receptors as well as the kinetic course of altered receptor expression

is mandatory. We developed an ET_AR specific photoprobe for the *in vivo* delineation of receptors by optical molecular imaging and recently used it for visualizing ET_AR-expression in tumor xenografts.[38-40] Here, we demonstrate the applicability of this probe for the evaluation and delineation of receptor distribution in a murine model of myocardial infarction.

Materials and Methods

General. All chemicals, reagents and solvents were analytical grade and purchased from commercial sources. The precursor compound benzo[1,3]dioxol-5-yl-3-(2-(2-(2-(2-amino-ethoxy)ethoxy)ethoxy)ethoxy)-4,5-dimethoxybenzyl-5-hydroxy-5-(4-methoxyphenyl)-5H-furan-2-one was synthesized as described before. The NHS ester of IRDye800cw was available from LICOR Biosciences (Lincoln, NE). Mass spectrometry of the final probe CH861 was performed using an Orbitrap LTQ XL (Thermo Scientific, Dreieich, Germany) spectrometer with nanospray capillary inlet. HPLC-purification was performed on a gradient RP-HPLC using a Knauer system with two K-1800 pumps, an S-2500 UV detector and a RP-HPLC Nucleosil 100-5 C18 column (250 mm × 8.0 mm). The recorded data was processed by the ChromGate HPLC software (Herbert Knauer GmbH, Berlin, Germany).

Probe. The applied probe CH861 is based on an already published small molecule fluorescent endothelin receptor antagonist.[38] For the present study, the fluorescent dye IRDye800cw - as NHS active ester - was coupled to the precursor amino compound. In brief, equal amounts of precursor PEG amine hydrochloride and dye active ester were dissolved in a 2:1 mixture of DMF and DMSO and 2% v/v DIPEA was added. After reaction at room temperature for 20 h the mixture was directly purified by HPLC (acetonitrile and water with 0.1% TFA with the following gradient: 1 min 90% water, then 15 min from 90% to 45%, then 2 min 45%, then 1 min from 45% to 90%, then 1 min 90%, overall 20 min, t_R = 14.4 min). MS (Orbitrap/ESI): m/z = 549.49026 $[M-3H]^{3-}$ (calc.: $C_{81}H_{90}N_3O_{26}S_4$ = 549.49039), 835.72954 $[M-3H+Na]^{2-}$ (calc.: $C_{81}H_{90}N_3O_{26}S_4Na$ = 835.73020).

Animals. All animal procedures and their care were conducted in conformity with national and international guidelines (EU 2010/63) with approval from the local authorities (Government of Upper Bavaria and Government of North Rhine Westphalia) and supervised by the respective Animal Care and Use Committee. Animals were housed in standard animal rooms (12 h light/dark cycle, 50-60% humidity, 18°C-23°C temperature, bedding material) in individually ventilated cage systems (IVS Techniplast) under specific pathogen-free conditions with free access to water and standard laboratory chow ad libitum. Myocardial infarction (MI) surgery was performed on female C57Bl/6J mice (aged 8-10 weeks, n = 32, Charles River Laboratories, Sulzfeld, Germany). Myocardial infarction was induced by

permanent ligation of the left anterior descending artery (LAD) as previously described.[41, 42] The animals were intubated orotracheally and mechanically ventilated. A left thoracotomy was performed in the fourth intercostal space, the pericardium was opened, and the left anterior descending artery ligated permanently with an 8.0 nylon suture (Ethicon, Norderstedt, Germany). After thoracotomy, subcutaneous tissue and skin were closed in separate layers and the animal weaned from the ventilator. Mice were anesthetized by injection anesthesia with MMF (Medetomidin, Midazolam, Fentanyl) and by inhalation anesthesia (isofluorane 1.5%–2.5% v/v in O_2) for surgical and imaging procedures. Analgesia was performed by preemptive subcutaneous application of buprenorphine and carprofen and was repeated every 12 hours until 72h hours after surgery. At indicated time points (day 1, day 7 and day 21 post surgery) mice received 2.0 or 4.0 nmol of CH861 dissolved in 100µl of saline as a bolus tail vein injection. After 4 hours of probe distribution mice were euthanized under deep anesthesia, and the hearts were excised and prepared for further *ex vivo* analysis. Hearts from healthy mice without MI (n = 6) were examined for comparison, as were infarcted hearts from mice that received 4.0 nmol of the pure dye IRDye800cw (n = 7). Mice for *in vivo* imaging (n = 5, see below) were given 4.0 nmol of the probe 7 days after surgery.

Cryoslicing/CCD imaging. After excision, hearts were washed with 0.9% NaCl and immediately frozen at -80°C. Before slicing the hearts via short axis, they were embedded vertically in optimal cutting temperature compound (OCT, TissueTek; Scene Acryl Black 906, Boesner). The slicing was performed using a CM1950 Leica rotary cryotome (Leica Microsystems GmbH, Wetzlar, Germany) equipped with a custom made imaging system.[43] The exposure time was automatically selected to ensure optimal use of the dynamic range of the EMCCD sensor. Every 200 µm fluorescent and color images were recorded. Episcopic images were evaluated using the analysis tool of the ImageJ software. A number of 4-5 distinct slices were measured. Regions of lower signal intensity were related to regions of higher intensity, yielding rough estimates of probe accumulation within the affected tissue. Above, around and in two areas below the ligation, sections of 20 µm thickness were collected for further histological and immunohistochemical analysis.

In vivo fluorescence mediated tomography (FMT). FMT studies were performed using the small-animal imaging system *FMT 2500* (PerkinElmer, Waltham, MA). Mice (n = 5) were shaved around the body at the region of interest and received 4.0 nmol of the probe as an i.v. injection via the tail vein 7 days post surgery. One healthy mouse without myocardial infarction was imaged as a control. Four hours after injection animals were placed inside the FMT imaging chamber under isoflurane anesthesia as described before.[39] Animal scan times were in the range of 2–5 min and image reconstruction times were about 1–3 min. Volumes

of interest were drawn around the heart region with the highest fluorochrome concentration close to the apex. The whole imaged region was used for comparison of probe concentration.

Ex vivo fluorescence reflectance imaging (FRI). Cryoslices of explanted hearts (n = 4) were placed inside the imaging chamber of the *In-Vivo FX PRO* Imaging System (Bruker Biospin MRI GmbH, Ettlingen, Germany). For imaging of the IRDye800cw-labeled probe, the excitation wavelength was set to 730 nm using an appropriate bandpass filter. Emission at 790 nm was recorded using a filter-equipped high-sensitivity (4-million-pixel) cooled charge-coupled device (CCD) camera. Acquisition time was 2 minutes for each image with a field of view (FOV) of 70x70mm. Using the manufacturers software, regions of interest (ROIs) were drawn around areas of putative infarction (recognized by HE staining of neighboring slides beforehand) and around remote areas of the same slide. Additionally, ROIs were placed inside slides of unaffected myocardial tissue for comparison. Additionally, healthy hearts (n = 4) without MI were processed accordingly.

Histology and immunofluorescence of cryosections. After drying and pre-fixation in 4% paraformaldehyde (PFA, Santa Cruz Biotechnology) cryosections were stained with hematoxylin and eosin according to the manufacturer's protocol (Morphisto). Further cryosections were stained for CD31 (DIA-310, Histonova), ET_AR (ab178454, Abcam), CD68-Alexa488 (ab201844, Abcam) and α-smooth muscle actin-FITC (F3777, Sigma). Fluorophore-coupled secondary antibodies at 594 nm and 488 nm wavelengths (LifeTechnologies) were used for visualization. The mounting media Prolong Diamond (LifeTechnologies) containing DAPI was used for tissue embedding and visualization of the cell nuclei. All slices were imaged using an Axio Imager M2 microscope (Carl Zeiss) equipped with the Zeiss Zen Pro 2.0 software (Carl Zeiss) or an Eclipse 50i microscope (Nikon) and NIS-Elements BS 3.22 software (Nikon).

Histology and immunohistochemistry (IHC) of FFPE sections. After excision, hearts (n = 4) were fixated in 4% neutral buffered formalin for 24 hours and subsequently embedded in paraffin according to standard protocols. Sections of 5µm thickness were then manufactured using a microtome (HM355S, Thermo Scientific). Sections were stained for ET_AR (ab178454, Abcam) as well as by hematoxylin and eosin (Morphisto) according to the manufacturer's protocol. All sections were scanned using the Aperio AT2 Scanner (Leica) and imaged using the Aperio Image Scope software (Leica). In addition, Elastica van Gieson (EvG) staining was performed according to the manufacturer's protocol (12739, Morphisto). Images from sections were recorded by an Eclipse 50i microscope (Nikon) and NIS-Elements BS 3.22 software (Nikon).

Data analysis and statistics. Images from cryoslicing/CCD imaging were evaluated using the analysis tool of ImageJ (1.49v). Gray values were corrected for exposure time to give comparable data (signal intensity per second, SI/s). Values are displayed as mean ± standard deviation. Data from FRI were collected and yielded fluorescence signal intensities (SI) from 0 to 20 absorption units (au). Data from four infarcted hearts (n = 54 slices) and 4 healthy hearts (n = 32 slices) were evaluated. A two-tailed t-test with *Welch* correction was performed to compare mean fluorescence signal intensity from infarcted and remote areas as well as from healthy hearts, using Prism 7.02 software (GraphPad). Significant differences were concluded from *p*-values < 0.05. Data are displayed as box plots with min-to-max whiskers. Levels of macrophage infiltration (from immunohistochemistry of CD68-positive cells) and collagen deposition (from EvG stainings) were evaluated by using Adobe Photoshop software CS2 (version 9.0) in combination with ImageJ. Briefly, CD68 expression was evaluated by separating RGB channels of section images and measuring regions of interest (ROIs) in the respective channel of infarcted hearts in comparison to sections from healthy hearts in ImageJ. Collagen deposits were evaluated by first selecting a red color range corresponding to high collagen amounts within Photoshop and extracting this range into a new file. Then this file was background subtracted by ImageJ and the mean gray values were measured. Significant differences were concluded from *p*-values < 0.05 (unpaired t-test). Data are displayed as columns with error bars (standard deviation).

Results

The ET_AR targeted fluoroprobe CH861 detects regions of ischemic injury.

Left anterior descending (LAD) artery occlusion led to defined myocardial infarction in all examined animals. Preliminary evaluation of infarcted hearts (n = 18) by cryoslicing combined with CCD fluorescent imaging revealed a distinct accumulation of CH861 in regions of ischemic injury. Differences between infarcted and remote myocardium could be observed for all time points (day 1, day 7 and day 21 post surgery), but were low when using the commonly applied amount of 2.0 nmol of probe per animal (**fig. 1a,c,e**). However, variances between time points were already visible. Especially at day 21 post surgery enhanced signal intensity was not only located in infarcted area adjacent to the border of the left ventricle, but also in remote regions (**fig. 1e**). Increasing the dose to 4.0 nmol per animal (≈ 250 µg/kg) clearly enhanced the differences in signal intensity at all time points examined (**fig. 1b,d,f**). As control, hearts of untreated animals without MI (n = 4) were evaluated using either CH861 (**fig. 1g**) or pure IRDye800cw (hydrolyzed @ 4.0 nmol, **fig. S1**), but regions of enhanced fluorescence could not be detected. Likewise, we applied the pure dye to MI

animals, which also resulted in an enhanced fluorescence in infarcted tissue at all time points examined (**fig. S1**), but the signal intensity was low compared to CH861 (see also **fig. 2b**). This signal can be attributed to unspecific extravasation of the dye within the inflammatory processes due to increased endothelial permeability.

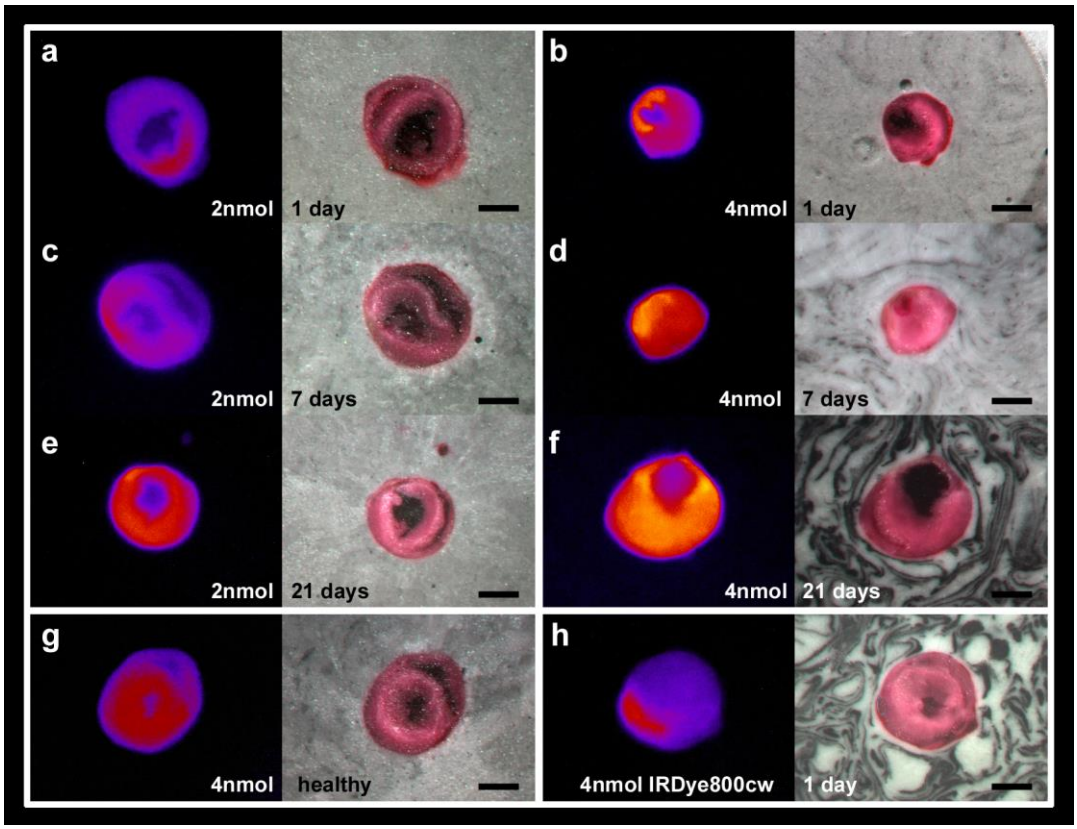

Figure 1: **Fluorescent images (pseudo-colored) and color photographs (RGB) of cryoslices during CCD imaging**. **a,c,e:** images of hearts 4 hours after injection of 2.0 nmol of CH861 at day 1 (**a**), day 7 (**c**) and day 21 (**e**) after surgery. **b,d,f:** images of hearts 4 hours after injection of 4.0 nmol of CH861 at day 1 (**b**), day 7 (**d**) and day 21 (**f**) after surgery. **g**: healthy heart 4 hours after injection of 4.0 nmol of CH861. **h**: infarcted heart 1 day after surgery and 4 hours after injection of 4.0 nmol of pure IRDye800cw (scale bar represents 2 mm).

The signal intensities (SI) of the cryoslices were evaluated by ImageJ software and standardized to exposure time (SI per second). Ratios of infarcted area to remote myocardium ranged from 1.17-1.22 in slices from animals injected with 2.0 nmol of the probe and from 1.42-1.66 in slices from the 4.0 nmol group. With only 2.0 nmol of the probe, differences between healthy and MI hearts could be observed, but were very low in terms of grey values. At day 7 after surgery we observed the highest signal intensity differences in affected tissue compared to remote myocardium in the 4.0 nmol group (**fig. 2a**) and therefore decided to add further experiments based on this setup. The control experiments with pure IRDye800cw also showed enhanced fluorescence intensity from infarcted regions, but with much lower SI (**fig. 2b**). Examination of healthy hearts with either of the probes likewise showed much lower intensity (**fig. 2c**).

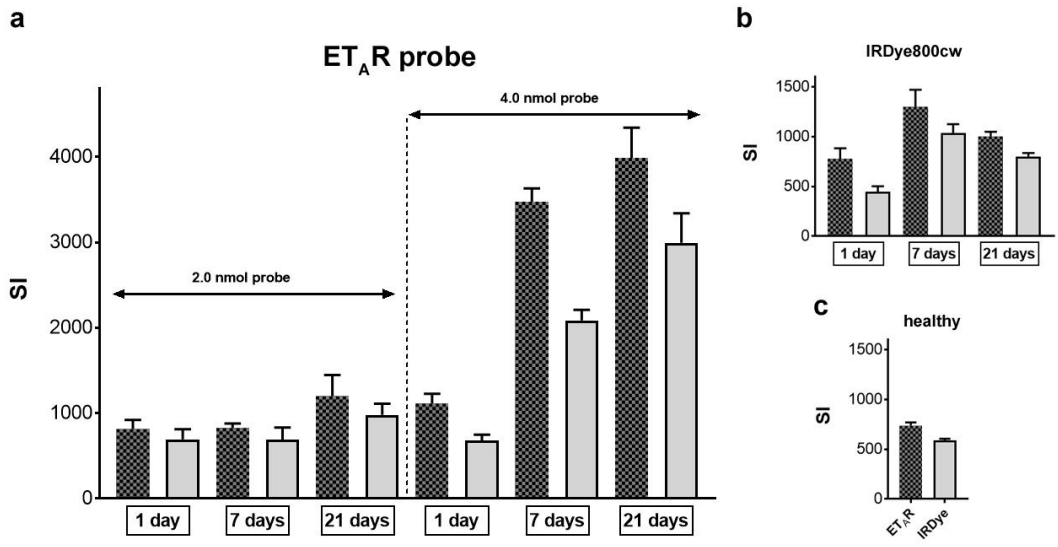

Figure 2: Evaluation of cryoslices of heart tissue. Signal intensities of slices from **a**. ET_AR probe treated mice (with the indicated amount) and **b**. IRDye800cw treated mice (4.0 nmol). Patterned bars display values of infarcted areas; solid bars display values of remote regions. **c**. Signal intensities of healthy tissue slices of mice treated with the ET_AR probe CH861 (patterned bar) and with pure IRDye800cw as a control (solid bar). All data are displayed as mean ± standard deviation per second of exposure time.

Since the technique of cryoslicing combined with fluorescent imaging collects photons from the whole residual tissue of the cryoconserved organ, and not from a single defined slice, a quantification of probe distribution is hardly feasible and signal enhancement can only be seen as an estimate of probe accumulation. Therefore, no statistical analysis was performed on these data.

In vivo imaging by FMT reveals high ET_AR signal intensity in the heart apex

To show the versatile applicability of our probe, we therefore decided to visualize infarcted hearts by FMT *in vivo*, which allows relative quantification of probe distribution inside specified regions/volumes of interest. At 4 hours after i.v. injection of the probe enhanced fluorescence intensity in the left anterior region of the chest was identified in all mice (**fig. 3a,b**). The relative accumulation of probe inside the drawn regions of interest (ROIs) at the apex region was 22-29% compared to whole probe amount inside the measured chest area. After organ removal post mortem, we imaged the isolated hearts again by FMT and could clearly visualize an area of high signal intensity at the apex region (**fig. 3c**). Control mice without MI did not show any enhanced fluorescence intensities for the ET_AR probe in the imaged chest area *in vivo*, nor did the explanted heart (**fig. 3d**).

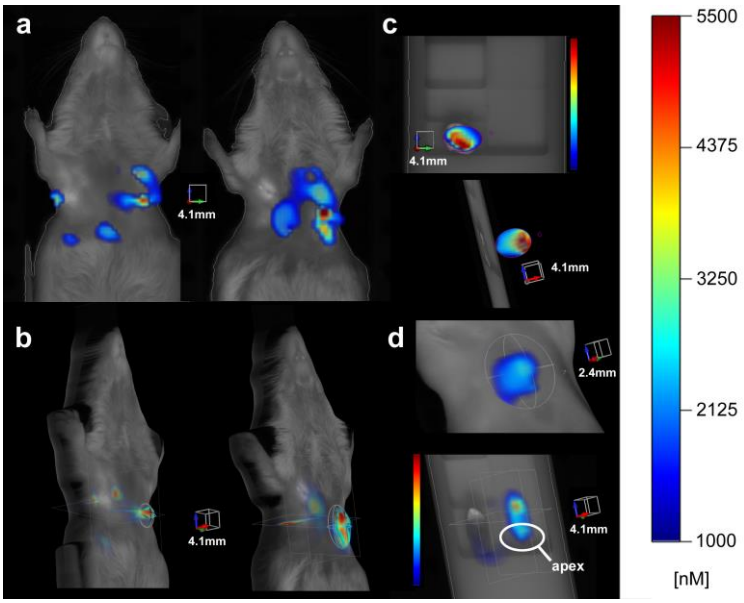

Figure 3: *In vivo* imaging of mice after MI by FMT. a. front view, two different mice **b.** side view with ROIs of the same mice. **c**. Explanted heart after MI showing areas of high SI in the apex region (front and side view). **d.** *in vivo* (top) and *ex vivo* image of a healthy heart revealing a lack of signal accumulation (color bar relates to *in vivo* images in **a,b,d**).

FRI enables evaluation of ET_AR signal intensities in tissue slices

Hearts from mice that underwent *in vivo* imaging were subsequently analyzed by FRI concerning probe distribution. This technique allows semi-quantitative evaluation of fluorescence intensities from cryoslices with a defined thickness prepared for e.g. microscopy. Slices were imaged and regions of high fluorescence were compared to regions of low SI (**fig. 4a**), including unaffected, more superior regions close to the base of the heart (**fig 4b**). Summarizing all examined hearts (n = 4) we analyzed 54 ROIs for infarcted regions and 54 ROIs for remote regions. We found significant differences in mean SI, 10.8 ± 0.6 au (au = absorption units) in infarcted areas, compared to a mean of 4.8 ± 0.4 au in remote areas ($p < 0.0001$). In addition, healthy hearts (**fig. 4c**, n = 4) were prepared in the same manner and quantified (n = 32 ROIs) to give a mean SI of 4.3 ± 0.5 au ($p < 0.0001$, **fig. 4d**).

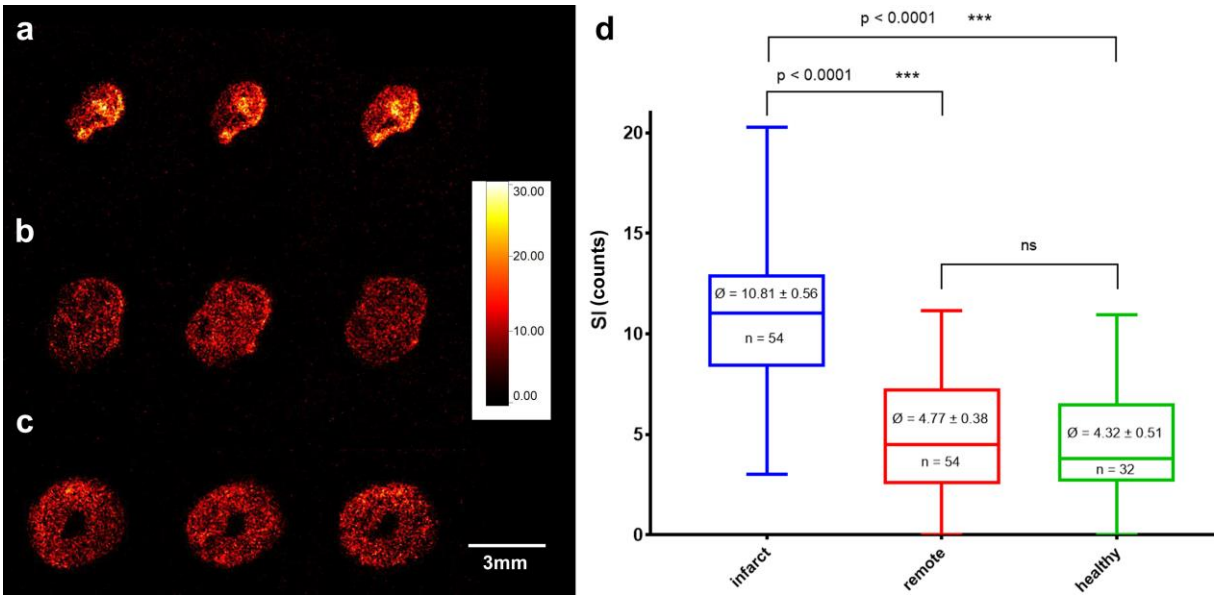

Figure 4: FRI evaluation of cryoslides. **a.** Examples of three consecutive slices of an infarcted heart (7 days post surgery) close to the apex with distinct regions of higher SI in regions of ischemic injury. **b.** Slices of an infarcted heart above the infarcted regions. **c.** Slices of a healthy heart. **d.** Quantification of cryoslides by FRI (box-plot min to max, numbers: mean ± SEM). Infarcted regions show a significantly higher SI than remote areas of the same hearts or healthy hearts (ns = not significant).

Localization of ET_AR and CH861 in infarcted myocardium

On the cellular level infarcted areas were identified by the examination of H&E stained sections. Morphological changes, as described for mouse hearts undergone MI, encompass ventricular wall thinning, chamber dilation, and the transition from necrosis to mature scar tissue.[44] At day 1 post surgery, affected regions showed large coagulative necrotic areas with signs of edema and leucocyte infiltration within the left ventricle wall (**fig. 5a, arrow**). Episcopic images (**fig. 5d-f**) corresponding to the H&E stained sections highlight the co-localization of probe with areas of pathological changes. After 7 days, infarcted regions can be located by a blueish color due to the replacement of cardiomyocytes with granulation tissue and ongoing inflammation (**fig. 5b, star**). After 21 days these areas are extended and the left ventricle is severely dilated (**fig. 5c, arrowhead**). The results were verified by immunofluorescence 7 days post surgery (**fig. S2**), showing a high number of CD68-positive cells, most likely macrophages, in the infarcted area as well as high amounts of collagen deposits as shown by Elastica van Gieson staining (**fig. S3**). The latter shows collagen deposits in large numbers within the infarcted areas, whereas the healthy control heart does not show domains of increased staining. Levels of increased CD68 expression and collagen deposition were evaluated and show significantly enhanced values in sections from infarcted hearts (**fig. S4**). The affected area correlates with the regions of high ET_AR fluorescence signal intensity from the initial cryoslicing/CCD imaging experiments (**fig. 5d-f**).

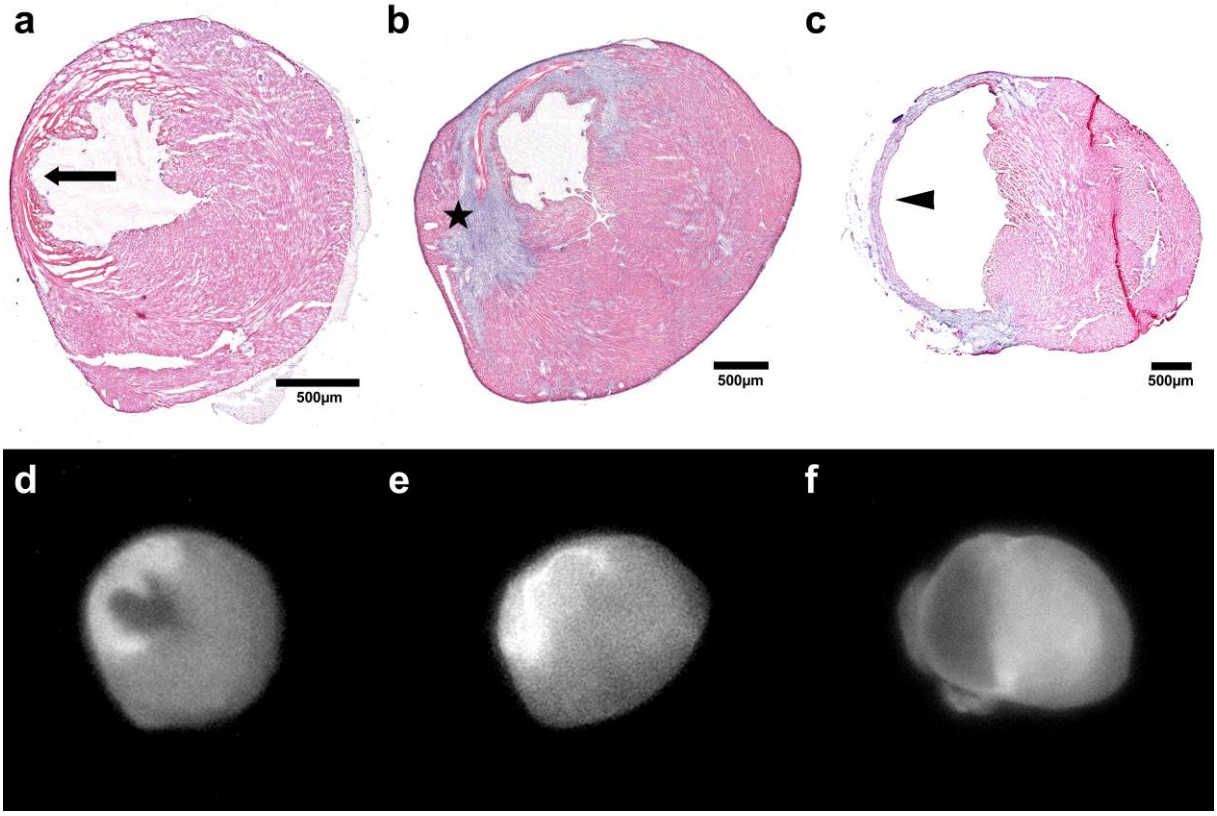

Figure 5: Accumulation of probe in infarct areas. H&E staining (**a-c**) and episcopic fluorescence imaging (**d-f)**, showing sections at day 1 (**a,d**), day 7 (**b,e**) and day 21 (**c,f**) post surgery. At all time points analyzed, probe accumulation is co-localized with infarcted areas and/or regions of remodeling processes. Arrow = necrotic area, star = inflammation, necrosis and fibrosis, arrowhead = dilated ventricle.

Subsequently, we performed ET_AR IHC (**fig. 6**) to follow the expression of ET_AR as target of the probe and further verify that the localization of the probe within infarcted tissue is correlated to high ET_AR abundance. In healthy hearts a low but uniform distribution of endothelin receptors throughout the myocardium can be found, located primarily at the cell membranes (**fig. 6a,c**). In the left ventricle wall of the infarcted heart (day 7 post surgery), a more intense staining for ET_AR is observed (**fig 6b**). ET_AR can be identified in a high number of small vessel structures (red arrows, **fig. 6d**), and also in intact cardiomyocytes (black arrows, **fig. 6d**). The analysis of ET_AR and CD31 expression of vessels inside the myocardium identified CD31-positive endothelial cells and ET_AR-positive cells in close proximity (**fig. S5**). This hints towards a contribution of ET_AR to angiogenic processes within the healing myocardium. Thus, our results support the importance of ET_AR-involvement in this mechanism as its expression is enhanced in infarcted areas. As the formation of new vessels is necessary for tissue repair, angiogenic factors emerge quite early after MI, leading to new vessel formation with only few days delay.[45, 46] Among these, vascular endothelial growth factor (VEGF) is the most prominent, which is known to be upregulated via ET-1/ET_AR-signaling.[47]

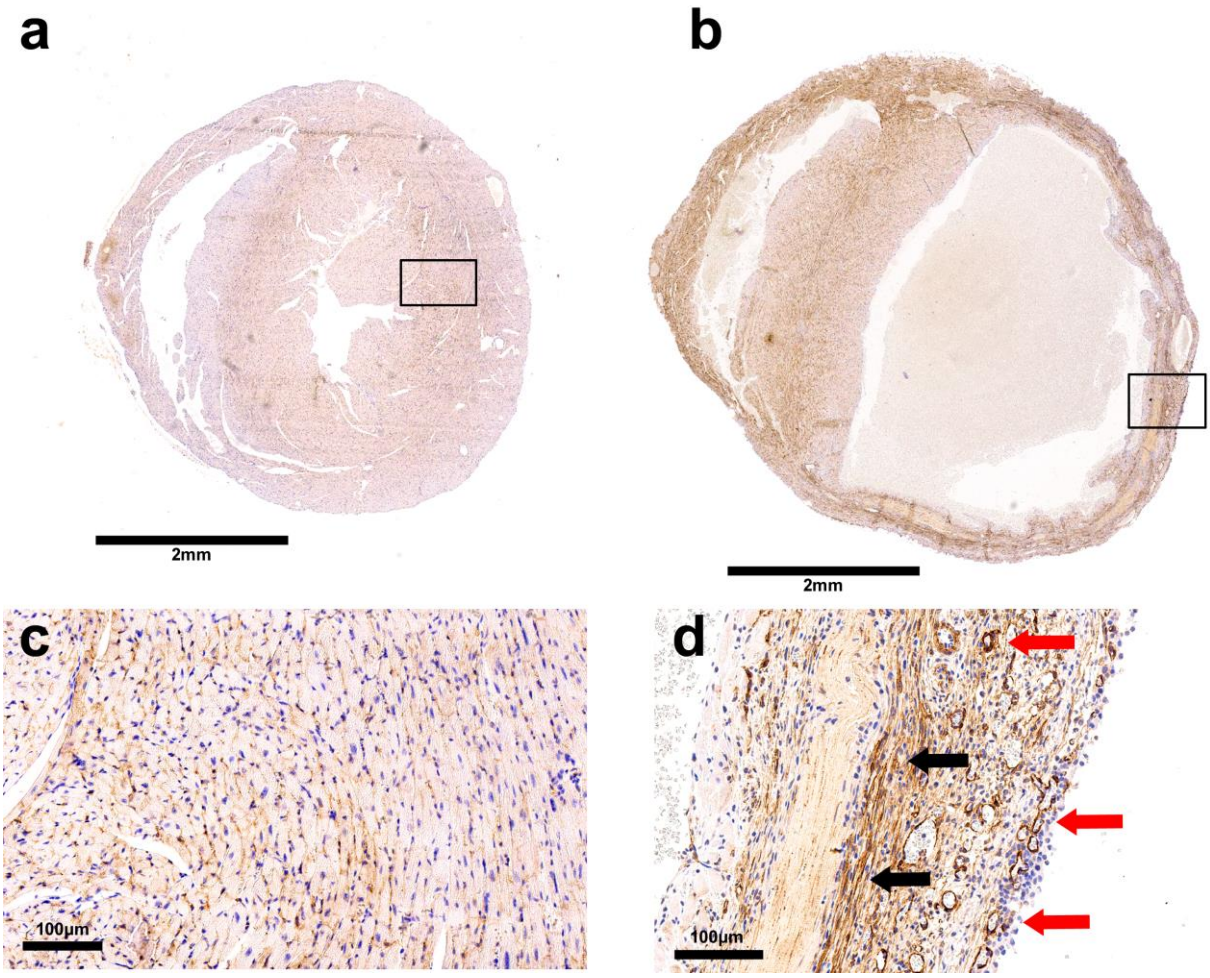

Figure 6: ET_AR expression in MI. IHC of a sham operated (**a, c**) and an infarcted heart day 7 post surgery (**b, d**). (**c**) Magnification of indicated area in (**a**). Peripheral membranous expression in myocytes can be observed. (**d**) Magnification of the left ventricle wall of the infarcted heart shown in (**b**). Increased ET_AR expression in cardiomyocytes and endothelial cells. Red arrows: vessels, black arrows: cardiomyocytes.

Discussion

The contribution of endothelin signaling to the pathophysiology of myocardial infarction in humans has first been investigated by Fukuchi and Giaid, who found distinct immunoreactivity for both ET-1 and endothelin converting enzyme (ECE-1) in macrophages that had accumulated in infarcted regions of ischemic tissue of cardiomyopathy patients.[48] Molecular imaging is an attractive means to evaluate druggable receptors in disease settings. Diagnosis using molecular imaging techniques allows non-invasive delineation of receptor expression and status and may show effects of therapy.[49] We herein show that a novel fluorescent probe targeting ET_AR is capable of delineating areas of high receptor density inside the infarcted area in *ex vivo* tissue examinations as well as *in vivo* with FMT in a mouse model of MI. The first build of the probe, labeled with Cy 5.5, showed favorable biodistribution and bioavailability in wild-type mice, including a balanced excretion route,

advantageous distribution and elimination half-lives and high specificity in myocardial tissue at the used time point.[50, 51] We do not expect substantial differences in distribution behavior applying IRDye800cw. This dye has the same amount of sulfonic acid groups as Cy 5.5 (four) to render the compound hydrophilic and therefore water soluble. The favorable excitation and emission profiles of IRDye800cw and its low toxicity have made this dye a widely used compound for preclinical optical molecular imaging applications as well as for clinical fluorescence-guided surgery interventions.[52, 53]

Recently, the utilization of a small molecular tracer for the imaging of ET receptor density in the rat heart after MI using positron emission tomography (PET) was introduced. Higuchi and colleagues developed an ^{18}F-labelled antagonist compound specific for ET_AR and showed its ability to image receptors in healthy rats *in vivo*. However, in contrast to our results presented here, the infarct area was not enhanced after MI, as shown by autoradiography. On the other hand, and in-line with our studies (**fig. 5 and 6**), they showed IHC clearly delineating localized ET_AR signal from the infarct zone and a positive correlation with CD31-staining, arguing that the signal originates from a small number of activated endothelial cells with strong ET_AR expression rather than from cardiomyocytes.[54] Both ET_AR and ET_BR are expressed within cardiac tissue, with ET_AR predominating on myocytes. However, ET_AR has only rarely been identified on endothelial cells; mouse renal glomerular endothelial cells (RGECs) express higher levels of ET_AR following renal ischemia/reperfusion injury and cultured human RGECs show increased ET-1 and ET_AR expression after induction of hypoxia.[55] Also, in patients with vascular disorders, enhanced ET-1 and ET_AR expression on endothelial cells was reported.[56]

In ischemic cardiomyopathy enhanced expression of ET_AR has been found by mRNA quantification of myocardial tissue and elevated ET-1 signaling through ET_AR is proposed to help maintain cardiac function.[57] Shortly after acute MI, a sudden loss of a high number of cardiomyocytes due to apoptosis and necrosis leads to an intense inflammation and in the formation of a firm collagen-based scar.[58] In our model of MI, post-ischemic inflammation was identified by CD68-positive macrophages in affected tissue and collagenous scar formation was revealed by Elastica van Gieson staining. Rat models of MI have identified the coincidence of elevated ET-1 levels with increased procollagen gene expression within the first week post MI.[27, 59] Cardiac fibroblasts express endothelin receptors and ET-1 signaling leads to increased collagen deposition and scar formation, which in turn prevents the thinning and expansion of the infarct zone. Therefore, an early enhancement of ET-1 and ET_AR expression is proposed to be beneficial for infarct healing.[60]

On the other hand, in animal models of heart failure, the benefit of long-term endothelin receptor antagonist treatment on survival has been described, with positive effects on

cardiac remodeling, including reduced cardiac hypertrophy and left ventricular collagen density, improved left ventricular contractility and increased left ventricular ejection fraction.[61, 62] So at later time points reduced ET-1/ET_AR signaling seems to promote beneficial remodeling processes. To understand and interpret these contradictory results, there is a strong need for more detailed comprehension of the role of ET receptors in the pathophysiology of MI.

The applied fluorescent probe CH861 shows promising results in this first proof of principle study. A further evaluation of the optimal time points for imaging or therapy is warranted and may enable a more detailed understanding of ET-axis contribution to post MI inflammation and remodeling. The limitations of our study result from the reduced translatability into clinical practice. While fluorescence guided surgery already found its way into tumor resection techniques in a number of cancers, e.g. glioma[63], prostate cancers[64] and hepatoblastoma[65], its applicability for vascular diseases is rather limited. Recently, intravascular catheter-based techniques have been introduced, which hold promise for future applications. [66-68] In contrast to PET-tracers, targeted probes for optical imaging have not yet been approved for human use. Only indocyanine green (ICG), fluorescein and methylene blue as unspecific perfusion-type probes have got an FDA approval. However, in view of future developments and the clinical need for new diagnostic and therapeutic approaches, fluorescence optical imaging and targeted optical probes may contribute to advancements in medical management of cardiovascular diseases.

Conclusion

With our developed probe we deliver a novel tool to gain dynamic insights into ET-axis engagement in cardiovascular disease, where its exact contribution is not yet well understood. Using a murine model of myocardial infarction, our preliminary experiments show that CH861 is capable of depicting ET_AR expression within the infarct area in *ex vivo* tissue examinations as well as *in vivo* by FMT. The observed differences in signal intensity from cryoslides of infarcted, remote and healthy myocardium in FRI are significant and suggest a relevant role for the endothelin axis in MI. Future investigations are necessary to validate this role, especially concerning time-course of enhanced receptor expression and signaling.

Associated Content

Supporting Information

The Supporting Information is available free of charge on the ACS Publications website at DOI:10.1021/acs.molpharmaceut.XXXX

Supplemental material: Additional histological images and histological data (PDF).

Acknowledgements

We thank Klaudia Niepagenkemper, Irina Arnhold and Dirk Reinhardt for excellent technical support. Also, we would like to thank Veronica Bodek for proof-reading. This study was funded in part by the Interdisciplinary Center for Clinical Research (IZKF) of the University of Münster (Vo2/014/09, PIX) and the German Research Foundation (DFG) *WI* 3686/4-1 and *ME* 3718/5-1. The authors declare that they have no conflict of interest.

References

1. Hickey, K. A.; Rubanyi, G.; Paul, R. J.; Highsmith, R. F. Characterization of a coronary vasoconstrictor produced by cultured endothelial cells. *The American journal of physiology* **1985,** *248*, (5 Pt 1), C550-6.

2. Yanagisawa, M.; Kurihara, H.; Kimura, S.; Tomobe, Y.; Kobayashi, M.; Mitsui, Y.; Yazaki, Y.; Goto, K.; Masaki, T. A novel potent vasoconstrictor peptide produced by vascular endothelial cells. *Nature* **1988,** *332*, (6163), 411-5.

3. Davenport, A. P.; Hyndman, K. A.; Dhaun, N.; Southan, C.; Kohan, D. E.; Pollock, J. S.; Pollock, D. M.; Webb, D. J.; Maguire, J. J. Endothelin. *Pharmacological reviews* **2016,** *68*, (2), 357-418.

4. Dhaun, N.; Webb, D. J. Endothelins in cardiovascular biology and therapeutics. *Nature reviews. Cardiology* **2019**.

5. Jankowich, M.; Choudhary, G. Endothelin-1 levels and cardiovascular events. *Trends in cardiovascular medicine* **2019**.

6. Kolettis, T. M.; Barton, M.; Langleben, D.; Matsumura, Y. Endothelin in coronary artery disease and myocardial infarction. *Cardiology in review* **2013,** *21*, (5), 249-56.

7. Stow, L. R.; Jacobs, M. E.; Wingo, C. S.; Cain, B. D. Endothelin-1 gene regulation. *FASEB journal : official publication of the Federation of American Societies for Experimental Biology* **2011,** *25*, (1), 16-28.

8. Watanabe, T.; Suzuki, N.; Shimamoto, N.; Fujino, M.; Imada, A. Endothelin in myocardial infarction. *Nature* **1990,** *344*, (6262), 114.

9. Falk, M.; Huhn, R.; Behmenburg, F.; Ritz-Timme, S.; Mayer, F. Biomechanical stress in myocardial infarctions: can endothelin-1 and growth differentiation factor 15 serve as immunohistochemical markers? *International journal of legal medicine* **2018,** *132*, (2), 509-518.

10. Miyauchi, T.; Yanagisawa, M.; Tomizawa, T.; Sugishita, Y.; Suzuki, N.; Fujino, M.; Ajisaka, R.; Goto, K.; Masaki, T. Increased plasma concentrations of endothelin-1 and big endothelin-1 in acute myocardial infarction. *Lancet* **1989,** *2*, (8653), 53-4.

11. Cernacek, P.; Stewart, D. J.; Monge, J. C.; Rouleau, J. L. The endothelin system and its role in acute myocardial infarction. *Canadian journal of physiology and pharmacology* **2003,** *81*, (6), 598-606.

12. Eitel, I.; Nowak, M.; Stehl, C.; Adams, V.; Fuernau, G.; Hildebrand, L.; Desch, S.; Schuler, G.; Thiele, H. Endothelin-1 release in acute myocardial infarction as a predictor of long-term prognosis and no-reflow assessed by contrast-enhanced magnetic resonance imaging. *American heart journal* **2010,** *159*, (5), 882-90.

13. Haaf, P.; Zellweger, C.; Reichlin, T.; Zbinden, A.; Wildi, K.; Mosimann, T.; Twerenbold, R.; Reiter, M.; Balmelli, C.; Freidank, H.; Gimenez, M. R.; Peter, F.; Freese, M.; Stelzig, C.; Hartmann, B.; Dinter, C.; Osswald, S.; Mueller, C. Utility of C-terminal proendothelin in the early diagnosis and risk stratification of patients with suspected acute myocardial infarction. *The Canadian journal of cardiology* **2014,** *30*, (2), 195-203.

14. Khan, S. Q.; Dhillon, O.; Struck, J.; Quinn, P.; Morgenthaler, N. G.; Squire, I. B.; Davies, J. E.; Bergmann, A.; Ng, L. L. C-terminal pro-endothelin-1 offers additional prognostic information in patients after acute myocardial infarction: Leicester Acute Myocardial Infarction Peptide (LAMP) Study. *American heart journal* **2007,** *154*, (4), 736-42.

15. Freixa, X.; Masotti, M.; Palomo, M.; Diaz-Ricart, M.; Escolar, G.; Guasch, E.; Regueiro, A.; Jimenez, M.; Betriu, A.; Heras, M. Endothelin-1 levels predict endothelial progenitor cell mobilization after acute myocardial infarction. *Microvascular research* **2011,** *82*, (2), 177-81.

16. Gao, R.; Wang, J.; Zhang, S.; Yang, G.; Gao, Z.; Chen, X. The Value of Combining Plasma D-Dimer and Endothelin-1 Levels to Predict No-Reflow After Percutaneous Coronary Intervention of ST-Segment Elevation in Acute Myocardial Infarction Patients with a Type 2 Diabetes Mellitus History. *Medical science monitor : international medical journal of experimental and clinical research* **2018,** *24*, 3549-3556.

17. Miyauchi, T.; Sakai, S. Endothelin and the heart in health and diseases. *Peptides* **2019,** *111*, 77-88.

18. Olivier, A.; Girerd, N.; Michel, J. B.; Ketelslegers, J. M.; Fay, R.; Vincent, J.; Bramlage, P.; Pitt, B.; Zannad, F.; Rossignol, P.; Investigators, E. Combined baseline and one-month changes in big endothelin-1 and brain natriuretic peptide plasma concentrations predict clinical outcomes in patients with left ventricular dysfunction after acute myocardial infarction: Insights from the Eplerenone Post-Acute Myocardial Infarction Heart Failure Efficacy and Survival Study (EPHESUS) study. *International journal of cardiology* **2017,** *241*, 344-350.

19. Fareh, J.; Touyz, R. M.; Schiffrin, E. L.; Thibault, G. Endothelin-1 and angiotensin II receptors in cells from rat hypertrophied heart. Receptor regulation and intracellular Ca2+ modulation. *Circulation research* **1996,** *78*, (2), 302-11.

20. Kaoukis, A.; Deftereos, S.; Raisakis, K.; Giannopoulos, G.; Bouras, G.; Panagopoulou, V.; Papoutsidakis, N.; Cleman, M. W.; Stefanadis, C. The role of endothelin system in cardiovascular disease and the potential therapeutic perspectives of its inhibition. *Current topics in medicinal chemistry* **2013,** *13*, (2), 95-114.

21. Pönicke, K.; Vogelsang, M.; Heinroth, M.; Becker, K.; Zolk, O.; Böhm, M.; Zerkowski, H. R.; Brodde, O. E. Endothelin receptors in the failing and nonfailing human heart. *Circulation* **1998,** *97*, (8), 744-51.

22. Zolk, O.; Quattek, J.; Sitzler, G.; Schrader, T.; Nickenig, G.; Schnabel, P.; Shimada, K.; Takahashi, M.; Bohm, M. Expression of endothelin-1, endothelin-converting enzyme, and endothelin receptors in chronic heart failure. *Circulation* **1999,** *99*, (16), 2118-23.

23. Takahashi, H.; Soma, S.; Muramatsu, M.; Oka, M.; Fukuchi, Y. Upregulation of ET-1 and its receptors and remodeling in small pulmonary veins under hypoxic conditions. *American journal of physiology. Lung cellular and molecular physiology* **2001,** *280*, (6), L1104-14.

24. Takahashi, H.; Soma, S.; Muramatsu, M.; Oka, M.; Ienaga, H.; Fukuchi, Y. Discrepant distribution of big endothelin (ET)-1 and ET receptors in the pulmonary artery. *The European respiratory journal* **2001,** *18*, (1), 5-14.

25. Pieske, B.; Beyermann, B.; Breu, V.; Loffler, B. M.; Schlotthauer, K.; Maier, L. S.; Schmidt-Schweda, S.; Just, H.; Hasenfuss, G. Functional effects of endothelin and regulation of endothelin receptors in isolated human nonfailing and failing myocardium. *Circulation* **1999,** *99*, (14), 1802-9.

26. Oie, E.; Clausen, O. P.; Yndestad, A.; Grogaard, H. K.; Attramadal, H. Endothelin receptor antagonism attenuates cardiomyocyte apoptosis after induction of ischemia in rats. *Scandinavian cardiovascular journal : SCJ* **2002,** *36*, (2), 108-16.

27. Oie, E.; Yndestad, A.; Robins, S. P.; Bornerheim, R.; Asberg, A.; Attramadal, H. Early intervention with a potent endothelin-A/endothelin-B receptor antagonist aggravates left ventricular remodeling after myocardial infarction in rats. *Basic research in cardiology* **2002,** *97*, (3), 239-47.

28. Pfeffer, J. M.; Finn, P. V.; Zornoff, L. A.; Pfeffer, M. A. Endothelin-A receptor antagonism during acute myocardial infarction in rats. *Cardiovascular drugs and therapy* **2000,** *14*, (6), 579-87.

29. Sakai, S.; Miyauchi, T.; Yamaguchi, I. Long-term endothelin receptor antagonist administration improves alterations in expression of various cardiac genes in failing myocardium of rats with heart failure. *Circulation* **2000,** *101*, (24), 2849-53.

30. Schneider, M. P.; Boesen, E. I.; Pollock, D. M. Contrasting actions of endothelin ET(A) and ET(B) receptors in cardiovascular disease. *Annual review of pharmacology and toxicology* **2007,** *47*, 731-59.

31. Gatzoulis, M. A.; Landzberg, M.; Beghetti, M.; Berger, R. M.; Efficace, M.; Gesang, S.; He, J.; Papadakis, K.; Pulido, T.; Galie, N.; Investigators, M. S. Evaluation of Macitentan in Patients With Eisenmenger Syndrome. *Circulation* **2019,** *139*, (1), 51-63.

32. De Haro, J.; Bleda, S.; Gonzalez-Hidalgo, C.; Michel, I.; Acin, F. Long-Term Effects of Bosentan on Cardiovascular Events in Hispanic Patients with Intermittent Claudication: Four-Year Follow-up of the CLAU Trial : The CLAU Randomized Trial Long-Term Outcome. *American journal of cardiovascular drugs : drugs, devices, and other interventions* **2019,** *19*, (2), 203-209.

33. Packer, M.; McMurray, J. J. V.; Krum, H.; Kiowski, W.; Massie, B. M.; Caspi, A.; Pratt, C. M.; Petrie, M. C.; DeMets, D.; Kobrin, I.; Roux, S.; Swedberg, K.; Investigators, E.; Committees. Long-Term Effect of Endothelin Receptor Antagonism With Bosentan on the Morbidity and Mortality of Patients With Severe Chronic Heart Failure: Primary Results of the ENABLE Trials. *JACC. Heart failure* **2017,** *5*, (5), 317-326.

34. Cleland, J. G. F.; Teerlink, J. R.; Davison, B. A.; Shoaib, A.; Metra, M.; Senger, S.; Milo, O.; Cotter, G.; Bourge, R. C.; Parker, J. D.; Jondeau, G.; Krum, H.; O'Connor, C. M.; Torre-Amione, G.; van Veldhuisen, D. J.; McMurray, J. J. V.; Investigators, V. Measurement of troponin and natriuretic peptides shortly after admission in patients with heart failure-does it add useful prognostic information? An analysis of the Value of Endothelin Receptor Inhibition with Tezosentan in Acute heart failure Studies (VERITAS). *European journal of heart failure* **2017,** *19*, (6), 739-747.

35. O'Connor, C. M.; Gattis, W. A.; Adams, K. F., Jr.; Hasselblad, V.; Chandler, B.; Frey, A.; Kobrin, I.; Rainisio, M.; Shah, M. R.; Teerlink, J.; Gheorghiade, M.; Randomized Intravenous TeZosentan Study, I. Tezosentan in patients with acute heart failure and acute coronary syndromes: results of the Randomized Intravenous TeZosentan Study (RITZ-4). *Journal of the American College of Cardiology* **2003,** *41*, (9), 1452-7.

36. Kohan, D. E.; Cleland, J. G.; Rubin, L. J.; Theodorescu, D.; Barton, M. Clinical trials with endothelin receptor antagonists: what went wrong and where can we improve? *Life sciences* **2012,** *91*, (13-14), 528-39.

37. Ataya, A.; Cope, J.; Alnuaimat, H. A Review of Targeted Pulmonary Arterial Hypertension-Specific Pharmacotherapy. *Journal of clinical medicine* **2016,** *5*, (12).

38. Höltke, C.; von Wallbrunn, A.; Kopka, K.; Schober, O.; Heindel, W.; Schäfers, M.; Bremer, C. A fluorescent photoprobe for the imaging of endothelin receptors. *Bioconjugate chemistry* **2007,** *18*, (3), 685-94.

39. Büther, K.; Compeer, M. G.; De Mey, J. G.; Schober, O.; Schäfers, M.; Bremer, C.; Riemann, B.; Höltke, C. Assessment of endothelin-A receptor expression in subcutaneous and orthotopic thyroid carcinoma xenografts in vivo employing optical imaging methods. *Endocrinology* **2012,** *153*, (6), 2907-18.

40. Hahnenkamp, A.; Alsibai, W.; Bremer, C.; Höltke, C. Optimizing the bioavailability of small molecular optical imaging probes by conjugation to an albumin affinity tag. *Journal of controlled release : official journal of the Controlled Release Society* **2014,** *186*, 32-40.

41. Wildgruber, M.; Bielicki, I.; Aichler, M.; Kosanke, K.; Feuchtinger, A.; Settles, M.; Onthank, D. C.; Cesati, R. R.; Robinson, S. P.; Huber, A. M.; Rummeny, E. J.; Walch, A. K.; Botnar, R. M. Assessment of myocardial infarction and postinfarction scar remodeling with

an elastin-specific magnetic resonance agent. *Circulation. Cardiovascular imaging* **2014,** *7*, (2), 321-9.

42. Kuhlmann, M. T.; Kirchhof, P.; Klocke, R.; Hasib, L.; Stypmann, J.; Fabritz, L.; Stelljes, M.; Tian, W.; Zwiener, M.; Mueller, M.; Kienast, J.; Breithardt, G.; Nikol, S. G-CSF/SCF reduces inducible arrhythmias in the infarcted heart potentially via increased connexin43 expression and arteriogenesis. *The Journal of experimental medicine* **2006,** *203*, (1), 87-97.

43. Sarantopoulos, A.; Themelis, G.; Ntziachristos, V. Imaging the bio-distribution of fluorescent probes using multispectral epi-illumination cryoslicing imaging. *Molecular imaging and biology : MIB : the official publication of the Academy of Molecular Imaging* **2011,** *13*, (5), 874-85.

44. Virag, J. A.; Rolle, M. L.; Reece, J.; Hardouin, S.; Feigl, E. O.; Murry, C. E. Fibroblast growth factor-2 regulates myocardial infarct repair: effects on cell proliferation, scar contraction, and ventricular function. *The American journal of pathology* **2007,** *171*, (5), 1431-40.

45. Nahrendorf, M.; Swirski, F. K. Monocyte and macrophage heterogeneity in the heart. *Circulation research* **2013,** *112*, (12), 1624-33.

46. Swirski, F. K.; Nahrendorf, M. Imaging macrophage development and fate in atherosclerosis and myocardial infarction. *Immunology and cell biology* **2013,** *91*, (4), 297-303.

47. Lee, E. J.; Hwang, I.; Kim, G. H.; Moon, D.; Kang, S. Y.; Hwang, I. C.; Lee, S. Y.; Marie, P. J.; Kim, H. S. Endothelin-1 Augments Therapeutic Potency of Human Mesenchymal Stem Cells via CDH2 and VEGF Signaling. *Mol Ther-Meth Clin D* **2019,** *13*, 503-511.

48. Fukuchi, M.; Giaid, A. Expression of endothelin-1 and endothelin-converting enzyme-1 mRNAs and proteins in failing human hearts. *Journal of cardiovascular pharmacology* **1998,** *31 Suppl 1*, S421-3.

49. Curley, D.; Lavin Plaza, B.; Shah, A. M.; Botnar, R. M. Molecular imaging of cardiac remodelling after myocardial infarction. *Basic research in cardiology* **2018,** *113*, (2), 10.

50. Höltke, C.; Waldeck, J.; Kopka, K.; Heindel, W.; Schober, O.; Schäfers, M.; Bremer, C. Biodistribution of a nonpeptidic fluorescent endothelin A receptor imaging probe. *Molecular imaging* **2009,** *8*, (1), 27-34.

51. Mücke, M. M.; Bettenworth, D.; Geyer, C.; Schwegmann, K.; Poremba, C.; Schäfers, M.; Domagk, D.; Höltke, C.; Lenz, P. Targeting Mucosal Endothelin-A-Receptor Expression by Fluorescence Endoscopy is Feasible to Detect and Characterize Colitis-Associated Cancer in Mice. *Inflammatory bowel diseases* **2017,** *24*, (1), 111-122.

52. Chen, Y.; Pullambhatla, M.; Banerjee, S. R.; Byun, Y.; Stathis, M.; Rojas, C.; Slusher, B. S.; Mease, R. C.; Pomper, M. G. Synthesis and biological evaluation of low molecular weight fluorescent imaging agents for the prostate-specific membrane antigen. *Bioconjugate chemistry* **2012,** *23*, (12), 2377-85.

53. van Keulen, S.; Nishio, N.; Fakurnejad, S.; Birkeland, A.; Martin, B. A.; Lu, G.; Zhou, Q.; Chirita, S. U.; Forouzanfar, T.; Colevas, A. D.; van den Berg, N. S.; Rosenthal, E. L. The Clinical Application of Fluorescence-Guided Surgery in Head and Neck Cancer. *Journal of nuclear medicine : official publication, Society of Nuclear Medicine* **2019,** *60*, (6), 758-763.

54. Higuchi, T.; Rischpler, C.; Fukushima, K.; Isoda, T.; Xia, J.; Javadi, M. S.; Szabo, Z.; Dannals, R. F.; Mathews, W. B.; Bengel, F. M. Targeting of endothelin receptors in the healthy and infarcted rat heart using the PET tracer 18F-FBzBMS. *Journal of nuclear medicine : official publication, Society of Nuclear Medicine* **2013,** *54*, (2), 277-82.

55. Niu, J.; Wu, J.; Li, X.; Zhang, F. Association between endothelin-1/endothelin receptor A and inflammation in mouse kidneys following acute ischemia/reperfusion. *Molecular medicine reports* **2015,** *11*, (5), 3981-7.

56. Sek, A. C.; Xie, Z.; Terai, K.; Long, L. M.; Nelson, C.; Dudek, A. Z.; Druey, K. M. Endothelial Expression of Endothelin Receptor A in the Systemic Capillary Leak Syndrome. *PloS one* **2015,** *10*, (7), e0133266.

57. Serneri, G. G.; Cecioni, I.; Vanni, S.; Paniccia, R.; Bandinelli, B.; Vetere, A.; Janming, X.; Bertolozzi, I.; Boddi, M.; Lisi, G. F.; Sani, G.; Modesti, P. A. Selective upregulation of cardiac endothelin system in patients with ischemic but not idiopathic dilated cardiomyopathy: endothelin-1 system in the human failing heart. *Circulation research* **2000,** *86*, (4), 377-85.

58. Frangogiannis, N. G. Regulation of the inflammatory response in cardiac repair. *Circulation research* **2012,** *110*, (1), 159-73.

59. Tzanidis, A.; Lim, S.; Hannan, R. D.; See, F.; Ugoni, A. M.; Krum, H. Combined angiotensin and endothelin receptor blockade attenuates adverse cardiac remodeling post-myocardial infarction in the rat: possible role of transforming growth factor beta(1). *Journal of molecular and cellular cardiology* **2001,** *33*, (5), 969-81.

60. Adlbrecht, C.; Wurm, R.; Humenberger, M.; Andreas, M.; Redwan, B.; Distelmaier, K.; Klappacher, G.; Lang, I. M. Peri-interventional endothelin--a receptor blockade improves long-term outcome in patients with ST-elevation acute myocardial infarction. *Thrombosis and haemostasis* **2014,** *112*, (1), 176-82.

61. Mishima, T.; Tanimura, M.; Suzuki, G.; Todor, A.; Sharov, V. G.; Goldstein, S.; Sabbah, H. N. Effects of long-term therapy with bosentan on the progression of left ventricular dysfunction and remodeling in dogs with heart failure. *Journal of the American College of Cardiology* **2000,** *35*, (1), 222-9.

62. Sakai, S.; Miyauchi, T.; Kobayashi, M.; Yamaguchi, I.; Goto, K.; Sugishita, Y. Inhibition of myocardial endothelin pathway improves long-term survival in heart failure. *Nature* **1996,** *384*, (6607), 353-5.

63. Hadjipanayis, C. G.; Stummer, W.; Sheehan, J. P. 5-ALA fluorescence-guided surgery of CNS tumors. *Journal of neuro-oncology* **2019,** *141*, (3), 477-478.

64. Derks, Y. H. W.; Lowik, D.; Sedelaar, J. P. M.; Gotthardt, M.; Boerman, O. C.; Rijpkema, M.; Lutje, S.; Heskamp, S. PSMA-targeting agents for radio- and fluorescence-guided prostate cancer surgery. *Theranostics* **2019,** *9*, (23), 6824-6839.

65. Yamada, Y.; Ohno, M.; Fujino, A.; Kanamori, Y.; Irie, R.; Yoshioka, T.; Miyazaki, O.; Uchida, H.; Fukuda, A.; Sakamoto, S.; Kasahara, M.; Matsumoto, K.; Fuchimoto, Y.; Hoshino, K.; Kuroda, T.; Hishiki, T. Fluorescence-Guided Surgery for Hepatoblastoma with Indocyanine Green. *Cancers* **2019,** *11*, (8).

66. Matthews, S. D.; Frishman, W. H. A Review of the Clinical Utility of Intravascular Ultrasound and Optical Coherence Tomography in the Assessment and Treatment of Coronary Artery Disease. *Cardiology in review* **2017,** *25*, (2), 68-76.

67. Uchida, T.; Hamasaki, A.; Kuroda, Y.; Yamashita, A.; Sadahiro, M. Surgical management of proximal coronary arteriovenous fistulas using intraoperative fluorescence imaging. *Journal of cardiac surgery* **2018,** *33*, (12), 836-839.

68. Calfon Press, M. A.; Mallas, G.; Rosenthal, A.; Hara, T.; Mauskapf, A.; Nudelman, R. N.; Sheehy, A.; Polyakov, I. V.; Kolodgie, F.; Virmani, R.; Guerrero, J. L.; Ntziachristos, V.; Jaffer, F. A. Everolimus-eluting stents stabilize plaque inflammation in vivo: assessment by intravascular fluorescence molecular imaging. *European heart journal cardiovascular Imaging* **2017,** *18*, (5), 510-518.

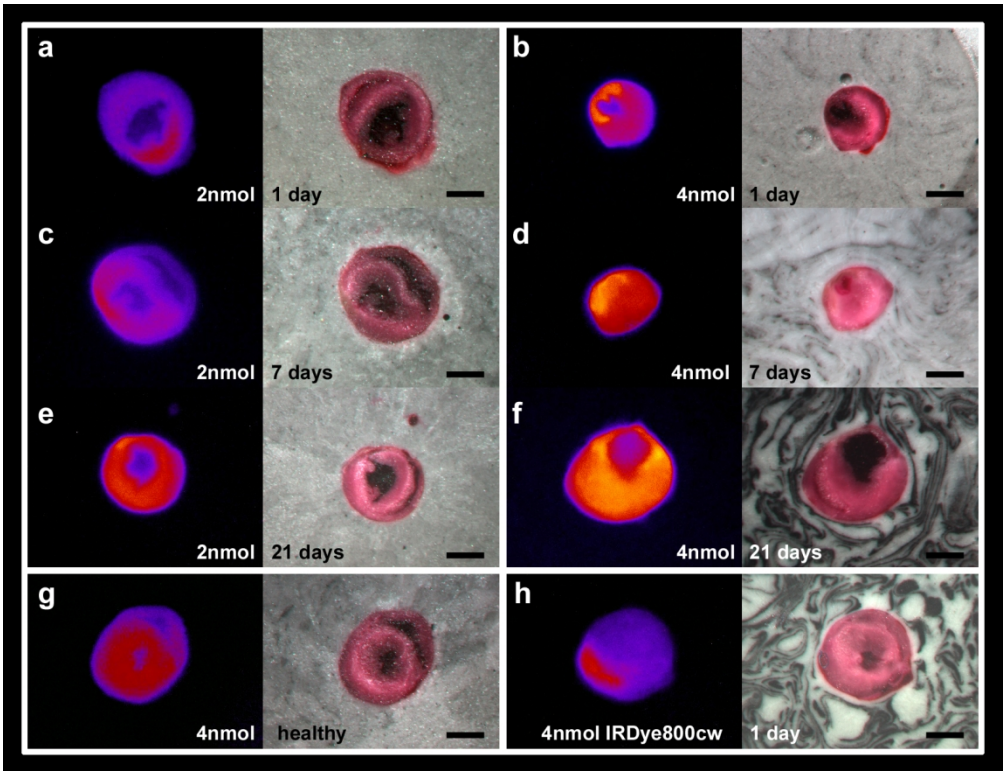

Figure 1: Fluorescent images (pseudo-colored) and color photographs (RGB) of cryoslices during CCD imaging. a,c,e: images of hearts 4 hours after injection of 2.0 nmol of CH861 at day 1 (**a**), day 7 (c) and day 21 (**e**) after surgery. **b,d,f**: images of hearts 4 hours after injection of 4.0 nmol of CH861 at day 1 (b), day 7 (d) and day 21 (f) after surgery. g: healthy heart 4 hours after injection of 4.0 nmol of CH861. **h**: infarcted heart 1 day after surgery and 4 hours after injection of 4.0 nmol of pure IRDye800cw (scale bar represents 2 mm).

141x108mm (300 x 300 DPI)

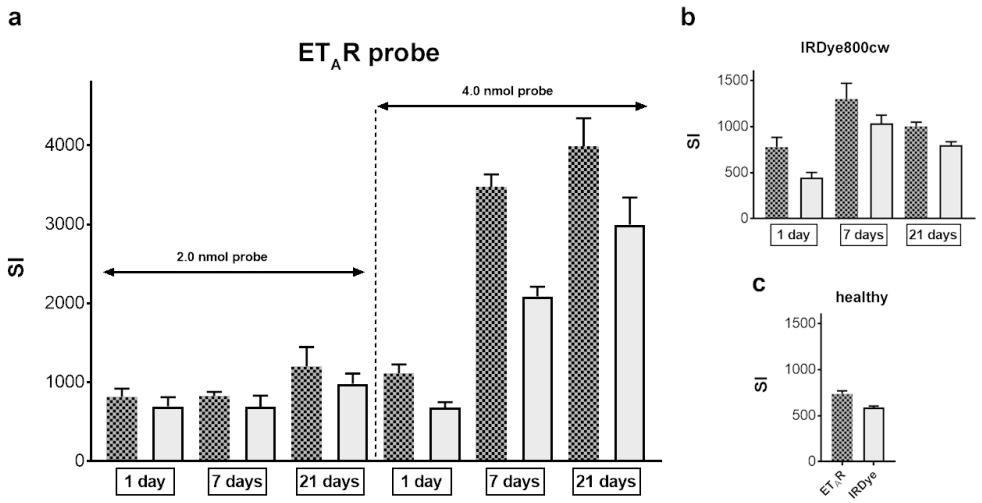

Figure 2: Evaluation of cryoslices of heart tissue. Signal intensities of slices from **a.** ET_AR probe treated mice (with the indicated amount) and **b.** IRDye800cw treated mice (4.0 nmol). Patterned bars display values of infarcted areas; solid bars display values of remote regions. **c.** Signal intensities of healthy tissue slices of mice treated with the ET_AR probe CH861 (patterned bar) and with pure IRDye800cw as a control (solid bar). All data are displayed as mean ± standard deviation per second of exposure time.

108x60mm (300 x 300 DPI)

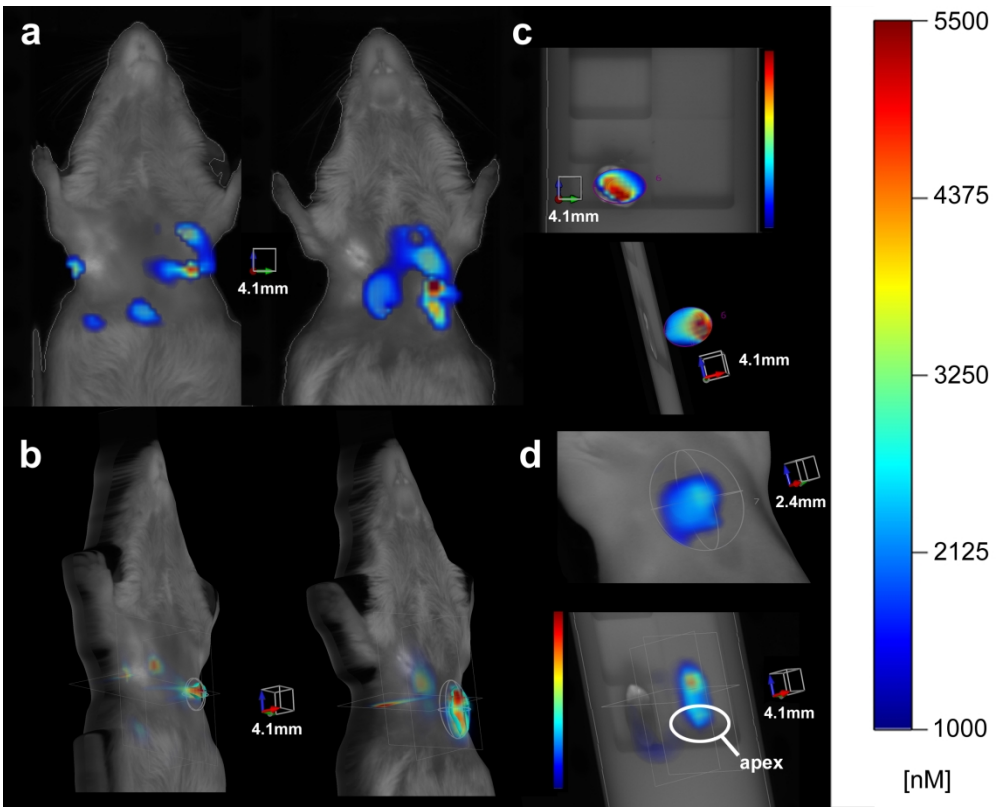

Figure 3: In vivo imaging of mice after MI by FMT. a. front view, two different mice b. side view with ROIs of the same mice. c. Explanted heart after MI showing areas of high SI in the apex region (front and side view). **d.** in vivo (top) and ex vivo image of a healthy heart revealing a lack of signal accumulation (color bar relates to in vivo images in **a,b,d**).

219x175mm (300 x 300 DPI)

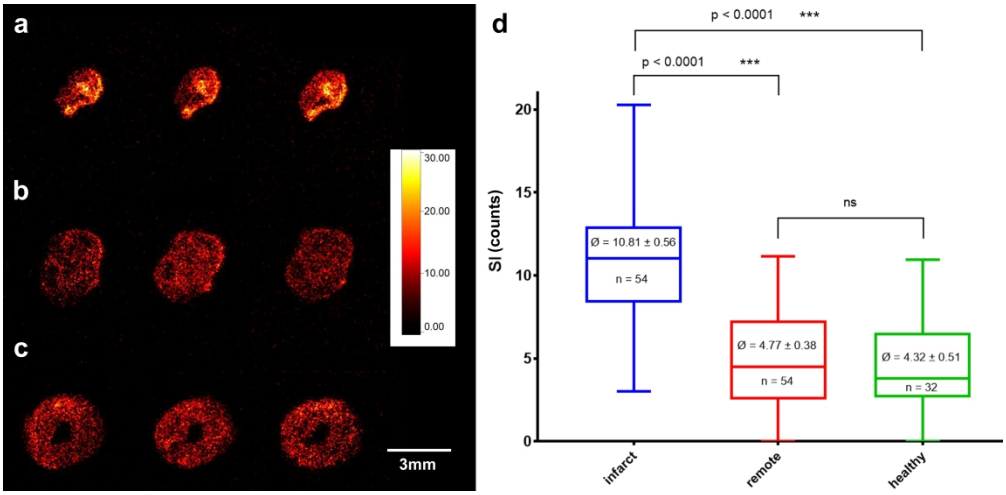

Figure 4: FRI evaluation of cryoslides. a. Examples of three consecutive slices of an infarcted heart (7 days post surgery) close to the apex with distinct regions of higher SI in regions of ischemic injury. b. Slices of an infarcted heart above the infarcted regions. c. Slices of a healthy heart. **d.** Quantification of cryoslides by FRI (box-plot min to max, numbers: mean ± SEM). Infarcted regions show a significantly higher SI than remote areas of the same hearts or healthy hearts (ns = not significant).

309x151mm (300 x 300 DPI)

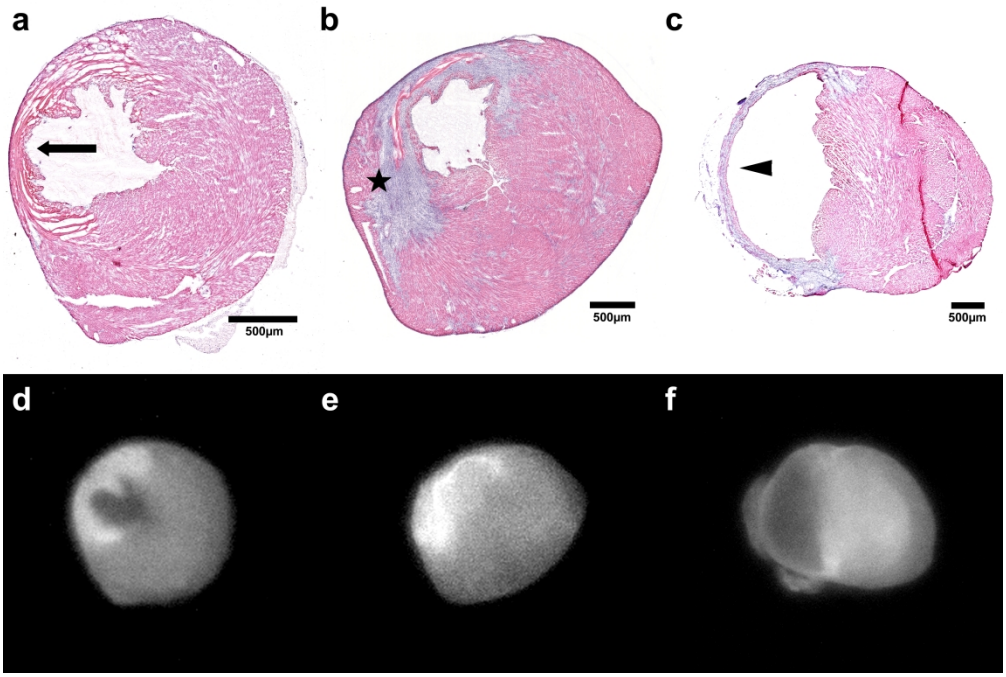

Figure 5: Accumulation of probe in infarct areas. H&E staining (**a-c**) and episcopic fluorescence imaging (**d-f**), showing sections at day 1 (**a,d**), day 7 (**b,e**) and day 21 (**c,f**) post surgery. At all time points analyzed, probe accumulation is co-localized with infarcted areas and/or regions of remodeling processes. Arrow = necrotic area, star = inflammation, necrosis and fibrosis, arrowhead = dilated ventricle.

520x351mm (300 x 300 DPI)

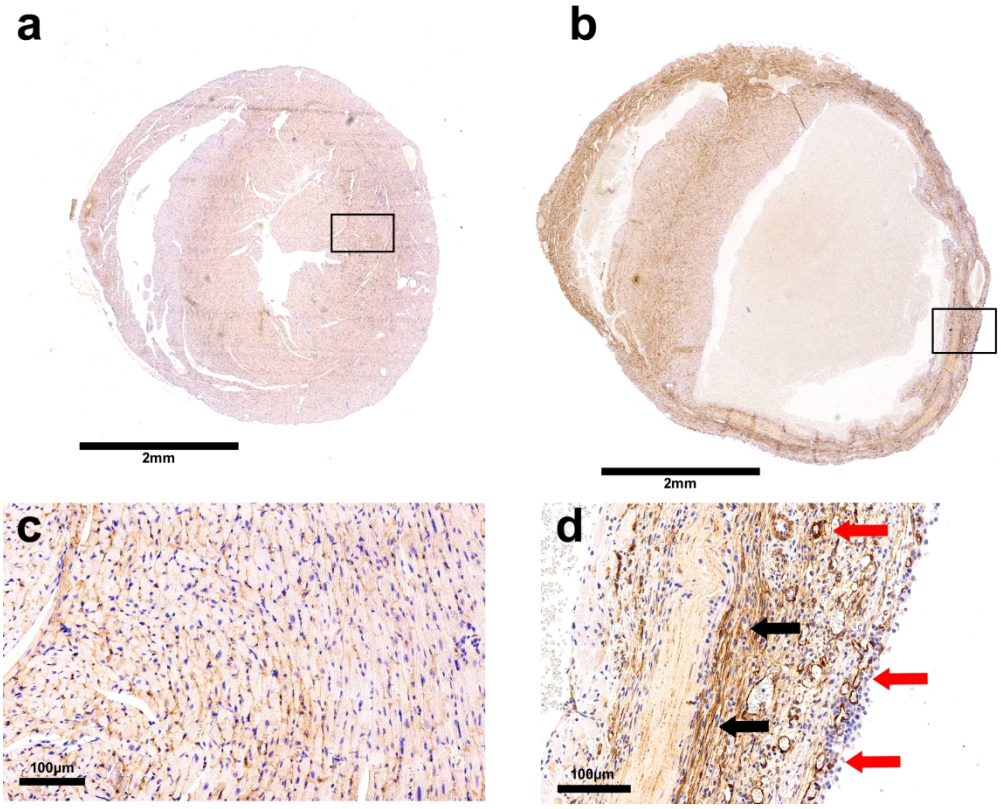

Figure 6: ET_AR expression in MI. IHC of a sham operated (**a, c**) and an infarcted heart day 7 post surgery (**b, d**). (**c**) Magnification of indicated area in (a). Peripheral membranous expression in myocytes. (d) Magnification of the left ventricle wall of the infarcted heart shown in (**b**). Increased ET_AR expression in myocytes and endothelial cells. Red arrows: vessels, black arrows: cardiomyocytes.

223x181mm (300 x 300 DPI)

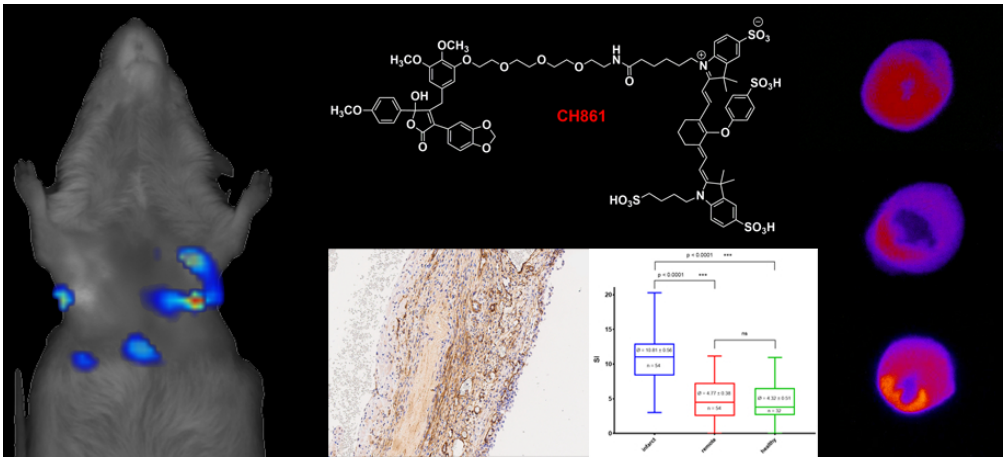

Table of Contents graphic

77x34mm (300 x 300 DPI)